Collisional shift and broadening of the $2p$-$2s$ spectral lines in muonic helium ions

G. Ya. Korenman,* V. N. Pomerantsev,† and V. P. Popov‡
Skobeltsyn Institute of Nuclear Physics, Lomonosov Moscow State University, 119234 Moscow, Russia
(Received 25 July 2013; published 9 September 2013)

In connection with the recently proposed Lamb-shift experiments at Paul Scherrer Institute in $\mu^4\mathrm{He}^+$ and $\mu^3\mathrm{He}^+$ by using the laser-spectroscopy method, the pressure shift and width of the $2p$-$2s$ spectral lines in muonic-helium ions were studied in the present paper within the fully quantum-mechanical close-coupling approach. The calculations of the S matrix as well as of the energy-dependent shift and width were made for collisional energies $E = 10^{-5}$–1 eV. The shift and width averaged over energy were obtained for target temperatures up to 350 K. It is shown that the fine-structure effect does not exceed a few percent. The isotopic effect is very small and can be neglected for the shift at $T \geqslant 150$ K, contrary to the width, for which the isotopic effect becomes much more pronounced at $T \geqslant 150$ K. At density $N = 2.4145 \times 10^{18}$ atom/cm^3 corresponding to the target pressure 100 mbar ($T = 300$ K) the predicted values of the shifts are equal to 35 (50) MHz for $\mu^3\mathrm{He}^+$ and 33 (35) MHz for $\mu^4\mathrm{He}^+$ respectively for upper (lower) values of the $2p$-$2s$ energy-level separation. At the same conditions the values of the widths are equal to 2.4 (13.6) MHz for $\mu^3\mathrm{He}^+$ and 2.0 (3.0) MHz for $\mu^4\mathrm{He}^+$.

DOI: 10.1103/PhysRevA.88.032503 PACS number(s): 36.10.−k, 32.70.Jz

I. INTRODUCTION

Low-energy muons entering the target form muonic atoms in highly excited states. The further evolution of their initial distributions in quantum numbers and kinetic energy are defined by the competition of the radiative and collisional-induced transitions as well as the elastic collisions during the atomic cascade. The lightest muonic atoms of the hydrogen and helium isotopes are of particular interest among the exotic atoms due to their simplest structure (quite similar to ordinary atoms but with an average size about two hundred times smaller) and provide unique opportunities for both theoretical and experimental investigations of a number of fundamental problems, such as physics of exotic atoms, quantum electrodynamics, weak interaction, and nuclear structure.

A special place in these studies belongs to experimental investigations of the metastable exotic atom states by means of laser-spectroscopy methods (e.g., see Ref. [1]) widely used in atomic physics. The crucial role for the feasibility of these and similar planned in PSI $\mu\mathrm{He}^+$ experiments [2,3] has a population and lifetime of the long-lived (metastable) $2s$ state formed during deexcitation cascade.

The arrival population of the $2s$ state in $\mu\mathrm{He}^+$ should be approximately the same as in the case of muonic hydrogen at very low target densities [4,5] since in both cases the deexcitation cascade is mainly dominated by the radiative transitions.

However, contrary to the muonic hydrogen case, the population of the metastable $2s$ state of $\mu\mathrm{He}^+$ is practically equal to the arrival population because of a strong suppression of the Coulomb deexcitation and fast thermalization of the muonic-helium ions due to long-range interatomic interaction. Thus, a few percent of the initially formed $\mu\mathrm{He}^+$ ions populate the long-lived $2s$ state and this value weakly depends on the density at a moderate pressure of the target gas [6]. Then a short laser pulse with a (tunable) wavelength corresponding to the $2p$-$2s$ energy level separation can induce the $2s \to 2p$ transition, which is immediately (0.5 ps) followed by $2p \to 1s$ radiative deexcitation. According to the proposal [2,3], the measurement of the transition frequencies with a precision of 50 ppm and their comparison with theoretical predictions will allow us to determine the root-mean-square charge radii of the nuclei ^{3,4}He with a relative accuracy 3×10^{-4} corresponding to 5×10^{-4} fm, that is an order of magnitude better than presently known.

For the proposed Lamb-shift laser experiments in $\mu^{3,4}\mathrm{He}^+$ [2,3] it would be also important to know the values of the pressure shift and broadening depending on the target density to choose a muon beam line with the corresponding target pressure. It is also important to be sure that there are no systematic shifts (uncertainties) of the $2p$-$2s$ frequencies due to the higher pressure, which does not allow us to reach the assumed accuracy about 5 GHz (1 eV corresponds to 241.79893 THz).

A schematic diagram of the energy levels for the first excited $n = 2$ states of $(\mu^4\mathrm{He})^+_{2l_j}$ is given in Fig. 1. The values of the Lamb shift and fine-structure splitting of the $2p$ energy level (spin-orbital splitting of the nl states due to the magnetic interaction between the orbital angular momentum l and spin $s = 1/2$ of the muon) are given according to Ref. [7].

In the case of $(\mu^3\mathrm{He})^+$ each of the $2l_j$ sublevels has also hyperfine structure (an additional splitting in total angular momentum $F = j \pm s_n$) due to magnetic interaction between angular momentum j of the muonic state and spin $s_n = 1/2$ of the ^{3}He nucleus. According to Ref. [7], a total energy splitting between $2p^F_j$ and $2s^{F'}_{1/2}$ sublevels varies from 1.119 eV to 1.460 eV depending on (j, F, F').

Muonic helium ions $(\mu^{3,4}\mathrm{He})^+$ formed in the deexcitation cascade are characterized by large values of the elastic and Stark mixing cross sections due to long-range polarization potential, therefore they are quickly thermalized before the laser pulse hits it. Thus, the kinetic energy distribution of the muonic-helium ions has to be the same as the energy distribution of the target atoms at given temperature.

*korenman@nucl-th.sinp.msu.ru
†pomeran@nucl-th.sinp.msu.ru
‡popov@nucl-th.sinp.msu.ru

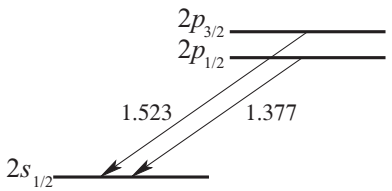

FIG. 1. Diagram of energy sublevels for muonic helium ion $(\mu^4\mathrm{He})^+_{2l_j}$. The values of the energy shift of the $2p_{1/2}$ and $2p_{3/2}$ sublevels relative to the $2s_{1/2}$ level are respectively equal to 1.377 eV and 1.523 eV [7].

A general quantum theory of the collisional shift and broadening of the spectral lines has been developed for the different pairs of the colliding subsystems and has been applied to numerous atomic and molecular systems (e.g., see Refs. [8,9] and references therein). It would be beneficial to apply this theory for the case of the muonic atoms (ions) collisions with the ordinary ones. According to our knowledge, in the case of the exotic atoms, this theory was only used for calculations of the shift and broadening of $E1$ [10,11] and $M1$ transitions [12,13] in antiprotonic helium atom, where the achieved experimental accuracy allows to discuss these values. Theoretical investigations of the collisional shift and broadening of the spectral lines $(2p\text{-}2s)$ for either $(\mu^3\mathrm{He})^+$ or $(\mu^4\mathrm{He})^+$ are of great interest since, as noted above, the knowledge of these effects for $(2p\text{-}2s)$ transitions in muonic helium ions might be important for the planning and interpretation of the Lamb-shift laser experiments.

In the present work we consider the collisional-induced shift and broadening of the spectral lines $2p \to 2s$ in $\mu^4\mathrm{He}^+$ and $\mu^3\mathrm{He}^+$ ions. In accordance with the general quantum theory, these values are expressed in terms of the S matrix for the collisions between muonic helium ions and ordinary helium atoms. In order to obtain the S matrix, we use a close-coupling approach, which was developed earlier by the authors and applied to exotic atom collisions in a number of papers (see, e.g., Refs. [5,14–19]).

The paper is organized as follows. A brief outline of the approach and interaction model are described in Sec. II. The results of the quantum-mechanical calculations of the collisional shifts and broadenings for the spectral lines $2p \to 2s$ in $\mu^4\mathrm{He}^+$ and $\mu^3\mathrm{He}^+$ ions are presented in Sec. III. Their energy and temperature dependencies are calculated at different values of the $2p\text{-}2s$ energy level separation for two variants: with and without taking into account fine-structure splitting. The main results of the paper are summarized in Sec. IV.

Atomic units ($\hbar = e = m_e = 1$) are used throughout the paper unless otherwise stated.

II. FORMALISM AND INTERACTION MODEL

The present study is based on a quantum-mechanical close-coupling description of the collisions. In the problem under consideration the kinetic energy of the relative ion-atomic motion is much smaller than the energy separation between the states of the muonic helium ion with the different principal quantum numbers n. Besides, the Lamb shift ($2s\text{-}2p$ energy separation) is about an order of magnitude more than the fine structure $2p_{3/2}\text{-}2p_{1/2}$ energy splitting and much larger than the hyperfine structure splitting in the case of the $(\mu^3\mathrm{He}^+)_{n=2}$. Hence, the states of the muonic helium ions with $n = 2$ are described in the present study in terms of the nonrelativistic hydrogenlike $2s$ and $2p$ orbitals. The energy of the $2s$ sublevel is shifted below on the value of the Lamb shift and summary Lamb and fine-structure shifts relative to the $2p_{1/2}$ and $2p_{3/2}$ sublevels, respectively. Therefore, the wave functions of the muonic helium states are defined by a vector coupling of the space hydrogenlike wave function $\phi_{nlm}(\mathbf{r}) = R_{nl}(r)Y_{lm}(\hat{\mathbf{r}})$ and muon spin function $\chi_{s\sigma}$:

$$\langle \mathbf{r}|nl,s:jm_j\rangle = R_{nl}(r)\sum_{m\sigma}\langle lms\sigma|jm_j\rangle Y_{lm}(\hat{\mathbf{r}})\chi_{s\sigma}. \quad (1)$$

Here, l, $s = 1/2$, and $j = l \pm 1/2$ are, respectively, the quantum numbers of the orbital, spin, and total muonic angular momentum; $\hat{\mathbf{r}} = \mathbf{r}/r$ and $\mathbf{r}$ is a radius vector of the muon relative to its nucleus.

The basis states are constructed from the wave functions of the muon $|nl,s:jm_j\rangle$ and the eigenfunctions $|L,\lambda\rangle$ of the angular momentum of the relative motion:

$$\langle \mathbf{r},\mathbf{R}|nlsj,L:JM\rangle = R_{nl}(r)\mathcal{Y}^{JM}_{lsj,L}(\hat{\mathbf{r}},\hat{\mathbf{R}}), \quad (2)$$

where

$$\mathcal{Y}^{JM}_{lsj,L}(\hat{\mathbf{r}},\hat{\mathbf{R}}) = \sum_{m\sigma\lambda m_j}\langle lms\sigma|jm_j\rangle\langle jm_jL\lambda|JM\rangle Y_{lm}(\hat{\mathbf{r}})Y_{L\lambda}(\hat{\mathbf{R}})\chi_{s\sigma}. \quad (3)$$

Here the total angular momentum $\mathbf{j}$ of the muonic state is coupled with the orbital momentum $\mathbf{L}$ of the relative motion to give the total angular momentum $\mathbf{J} = \mathbf{j} + \mathbf{L}$, and $\hat{\mathbf{R}} = \mathbf{R}/R$ with $\mathbf{R}$ is a radius vector, connecting the nucleus in the helium atom with the center-of-mass of the muonic helium ion.

The total wave function of the scattering problem at the total energy E and the definite quantum numbers of the total angular momentum (J,M) and parity $\pi = (-1)^{l+L}$ is expanded in terms of the basis states defined by Eqs. (2) and (3) as follows:

$$\Psi^{EJM\pi}(\mathbf{r},\mathbf{R}) = \frac{1}{R}\sum_{nljL}G^{EJ\pi}_{nljL}(R)|nlj,L:JM\rangle. \quad (4)$$

The expansion (4) leads to the close-coupling second-order differential equations for the radial functions $G^{EJ\pi}_{nljL}(R)$ of the relative motion:

$$\left(\frac{d^2}{dR^2} + k^2_{nlj} - \frac{L(L+1)}{R^2}\right)G^{EJ\pi}_{nljL}(R) = 2M_r\sum_{n'l'j'L'}W^{J\pi}_{nljL,n'l'j'L'}(R)\,G^{EJ\pi}_{n'l'j'L'}(R), \quad (5)$$

where $k^2_{nlj} = 2M_r(E_{\mathrm{cm}} - \Delta_{nlj,n_1j_1l_1})$ specifies the channel wave number; $M_r = M_1M_2/(M_1 + M_2)$ is a reduced mass of the colliding subsystems ($M_1 = M_Z + m_\mu$, $M_2 = M_Z + 2m_e$ denote the masses of the muonic helium ion and helium atom), where m_μ, m_e, and M_Z are the masses of the muon, electron, and the helium-isotope nucleus, respectively. In the present study we use the basis set in which both the open ($k^2_{nlj} > 0$) and closed ($k^2_{nlj} < 0, \mathrm{Im}\,k_{nlj} > 0$) channels were included. E_{cm} is the relative motion energy in the entrance $(n_1l_1j_1)$ channel

and $\Delta_{nlj,n_1l_1j_1}$ is the threshold of the current (nlj) channel referring to the entrance channel threshold:

$$\Delta_{nlj,n_1l_1j_1} = \varepsilon_{nlj} - \varepsilon_{n_1l_1j_1}. \quad (6)$$

Here ε_{nlj} is the bound-state energy for the (nlj) state of the muonic atom taking into account both the Lamb shift and fine-structure splitting.

The interaction potential matrix elements are given by

$$W^J_{c,c'}(R) = \langle nlj, L : JM|V(\mathbf{R},\mathbf{r})|nl'j', L' : JM\rangle, \quad (7)$$

where indexes c and c' denote the set of the channel quantum numbers: $c \equiv \{n,l,j,L\}$.

At a relative kinetic energy of 1 eV or less that we are interested in, the interaction $V(\mathbf{R},\mathbf{r})$ between an ordinary helium atom and muonic helium ion in the low-lying states with $n = 2$ can be introduced as a sum of two terms

$$V(\mathbf{R},\mathbf{r}) = V_0(R) + V_1(\mathbf{R},\mathbf{r}). \quad (8)$$

The first term $V_0(R)$ is assumed to be mainly the same as an adiabatic interaction potential of the point positively charged particle (proton) and helium atom except at very small separations [20,21]. As it will be shown in the next section (see below Figs. 3 and 4), the details of the interaction at separations $R \leqslant 0.8$ is unimportant in the scattering problem under consideration due to both a small Bohr radius of the $(\mu\mathrm{He}^+)_{n=2}$ $[n^2a_0/(Zm_\mu) \approx 5 \times 10^{-11}\mathrm{cm} \approx 0.01$ a.u.] and the extremely repulsive behavior of $V_0(R)$ (see Fig. 2). It is important to note that the difference in mass has no meaning with regard to the ground-state electronic wave function (and, hence, to the ground electronic state potential of the ion-atom pair) describing a helium atom in the external field of the positively charged particle and depending parametrically on the separation R between their center-of-mass. So, the ion-atomic potential $V_0(R)$ was chosen to be the same as the interatomic potential of $(\mathrm{H}^+ + \mathrm{He})$ obtained in highly accurate variational calculations [22] within the Born-Oppenheimer approximation. Since the results of the improved adiabatic calculations of the $(\mathrm{H}^+ + \mathrm{He})$ interatomic potential have been performed in Ref. [22] only at several points over a region R from 0.9 up to 6.0 a.u., we used in our study the data [23] (see the first and second columns of Table 1) derived from Ref. [22]. (Further in the text of the paper we will use the Refs. [22,23], taking account of the above remark.) At R values less than 0.9 a.u. we used the results of the approximate variational calculations [21] of the ground-state energy of $(\mathrm{HeH})^+$.

The proton-helium atom potential $V_0(R)$ evaluated in *ab initio* quantum-chemistry calculations [22,23] is plotted in Fig. 2. In the present paper this potential was analytically approximated by the sum of the short-range Morse potential $V_M(R)$ and long-range potential $V_p(R)$ (interaction between the point charge and the induced dipole on helium atom) as follows:

$$V_0(R) = V_M(R) + V_p(R), \quad (9)$$

where

$$V_M(R) = D_e(\{1 - \exp[-\beta(R - R_e)]\}^2 - 1), \quad (10)$$

$$V_p(R) = -\frac{\alpha_p}{2R^4}\, g(R), \quad (11)$$

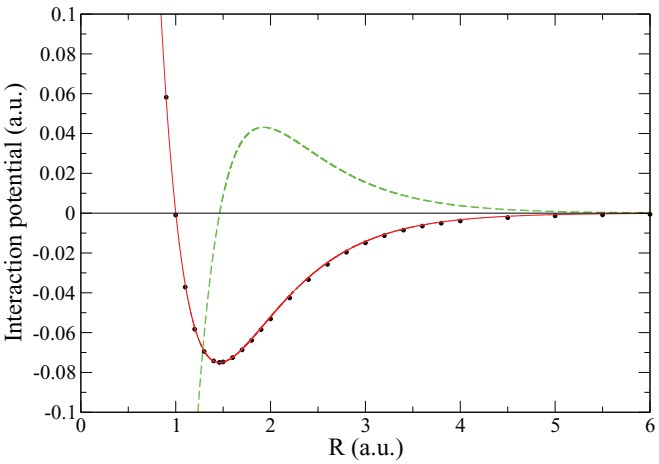

FIG. 2. (Color online) Interaction potential: central interatomic potential $V_0(R)$ (points are highly accurate adiabatic calculations [22,23], the solid line is the present fit by the sum of the Morse potential and long-range interaction (9)–(12); the dashed line is the R-depending factor $|I_r|\,\frac{dV_0(R)}{dR}$ (multiplied by 100 times) of the nondiagonal interaction in Eq. (17).

$$g(R) = \begin{cases} 0 & R < R_e, \\ 1 - \exp[-\gamma(R - R_e)^4], & R > R_e. \end{cases} \quad (12)$$

At the present fit the values of the well depth D_e, equilibrium separation R_e, and static dipole polarizability α_p of the He atom were fixed at their theoretical meanings: $D_e = 0.07493$, $R_e = 1.4632$ in accordance with [22], and $\alpha_p = 1.3837$ from Ref. [24]. Thus, only two free parameters β and γ, which determine the form of the Morse potential and cutoff function $g(R)$ of the long-range interaction $V_p(R)$, were fitted in the present study. As a result of the present fit (χ-square method was applied) we obtained $\beta = 1.489$ and $\gamma = 0.0035$ (all values are given in atomic units).

The results of analytical approximation (9)–(12) lead to very good agreement with the numerical values [22,23] of the interatomic potential over the whole range of R (see Fig. 2).

The second term in Eq. (8) is determined as the interaction of the dipole moment of $\mu\mathrm{He}^+$ with the electric field of the ordinary helium atom (with account of its polarization by the external field of the point charge of the $\mu\mathrm{He}^+$)

$$V_1(\mathbf{R},\mathbf{r}) = -\mathbf{d}\cdot\mathbf{E}(\mathbf{R}), \quad (13)$$

where, in accordance with the Hellmann-Feynman theorem, the electric field is given by

$$\mathbf{E} = -\nabla_{\mathbf{R}} V_0(R). \quad (14)$$

The interaction (13) results in the both dipole coupling of the channels and mixing of the $(\mu\mathrm{He})^+_{nlj}$ states ($2s$ and $2p$ in our study). The dipole moment operator of the muonic helium ion in its center-of-mass is given by

$$\mathbf{d} = -\xi\mathbf{r}, \quad (15)$$

where factor $\xi = (1 + m_\mu/M_1)$ arises due to the displacement of the center of charge against the center-of-mass in the muonic helium ion.

Then the interaction matrix (7) for the interaction potential $V(\mathbf{R},\mathbf{r})$ defined by (8)–(15) can be written as

$$W_{c,c'}(R) = V_0(R)\delta_{cc'} + W^{\rm dip}_{c,c'}(R), \tag{16}$$

where

$$W^{\rm dip}_{c,c'}(R) = (-1)^{J+1/2}\hat{l}\hat{l}'\hat{L}\hat{L}'\hat{j}\hat{j}'\langle l0l'0|10\rangle\langle L0L'0|10\rangle \times \begin{Bmatrix} l & l' & 1 \\ j' & j & 1/2 \end{Bmatrix}\begin{Bmatrix} L & L' & 1 \\ j' & j & J \end{Bmatrix} I_r \frac{dV_0(R)}{dR}. \tag{17}$$

Here $\hat{a} = \sqrt{2a+1}$, $\langle a0b0|c0\rangle$ is a Clebsch-Gordan coefficient, $\{\begin{smallmatrix} a & b & e \\ d & c & f \end{smallmatrix}\}$ is a $6j$ symbol, and

$$I_r = \xi\,\langle 2s|\,r\,|2p\rangle = -\frac{\xi\sqrt{3}}{M_{\mu\rm He}Z} \tag{18}$$

is a radial matrix element for the dipole moment operator of the muonic helium ion ($M_{\mu\rm He} = m_\mu M_Z/M_1$ is the reduced mass of the muonic helium ion in atomic units and $Z = 2$ is a charge of the nucleus). The R-depending factor $|I_r|\frac{dV_0(R)}{dR}$ (multiplied by 100 times) of the nondiagonal interaction in Eq. (17) is shown in Fig. 2.

Solving the system of coupled equations (5) for the radial functions of the relative motion $G_c(R)$ with the proper boundary conditions one can obtain the values for the S matrix defined in the subspace of the open channels. To find the S-matrix elements we use the propagator matrix method (for the details see Appendix A in Ref. [5]), which was employed in the recent calculations of the collisional quenching of the metastable $2s$ state in muonic hydrogen [5] and collision-induced absorption in hadronic atoms [18,19].

The obtained S-matrix elements are used to calculate the collisional shift $\tilde{d}(E)$ and broadening $\tilde{w}(E)$ of the $E1$ spectral lines ($2p_j \to 2s_{1/2}$) in the muonic helium ion as a function of the kinetic energy $E_{\rm cm}$ applying a general theory of the similar effects in atoms. In the case of the isolated lines (nonoverlapping levels) relevant to the problem under consideration, the collisional shift and broadening can be defined by means of the equation (59.98) from Ref. [8], which, in the present designations, takes the form

$$\begin{aligned} i\tilde{d}(E) + \frac{\tilde{w}(E)}{2} &= N\frac{\pi}{M_r^2}\sqrt{\frac{M_r}{2E}}\sum_{LL'J_iJ_f}(-1)^{L+L'} \\ &\times (2J_i+1)(2J_f+1)\begin{Bmatrix} J_f & J_i & 1 \\ j_i & j_f & L \end{Bmatrix}\begin{Bmatrix} J_f & J_i & 1 \\ j_i & j_f & L' \end{Bmatrix} \\ &\times [\delta_{LL'} - \langle j_iL'|S^{J_i}(E_i)|j_iL\rangle\langle j_fL'|S^{J_f}(E_f)|j_fL\rangle^*], \end{aligned} \tag{19}$$

where N is the target density and $\langle j_iL'|S^{J_i}(E_i)|j_iL\rangle$ is a scattering matrix element in the coupled $|jLJ\rangle$ representation. The elements of the S matrix in Eq. (19) correspond to the identical kinetic energies $E_{\rm cm}$ in the initial (i) and final (f) channels and therefore to different total energies of the system before and after the collision: $E_i = E_{\rm cm} + \varepsilon_{2l_ij_i}$ and $E_f = E_{\rm cm} + \varepsilon_{2l_fj_f}$, respectively. So the system of coupled equations (5) must be solved for each total angular momentum and parity as many times as there are different thresholds in the multichannel scattering problem, i.e., three times in the general case for our problem.

The averaged values for collisional broadening w and shift d at a definite target temperature T are obtained by averaging (19) over energy with the Maxwellian energy distribution of the target atoms:

$$id + \frac{w}{2} = \int_0^\infty F(E;T)\left[i\tilde{d}(E) + \frac{\tilde{w}(E)}{2}\right]dE, \tag{20}$$

where $F(E;T)$ is the normalized Maxwellian energy distribution of the target atoms

$$F(E;T) = \frac{2}{\sqrt{\pi}}(k_BT)^{-3/2}\sqrt{E}\exp[-E/(k_BT)], \tag{21}$$

(k_B is the Boltzmann constant).

III. RESULTS

Close-coupling calculations were performed in the relative energy range from 10^{-5} up to 1 eV (600 values in the whole range of the energy) until the convergence over partial waves was reached at given energy. The present calculations required about 70 partial waves at the highest energy. In addition, the distance at which the solutions can be safely treated as the free-field solutions was also determined numerically. The temperature dependencies of the widths and shifts were calculated at 0.5 K intervals in the range $T = 1$–350 K. In all present calculations the value of the target density $N = 2.4145 \times 10^{18}$ atom/cm^3 corresponding to the target pressure 100 mbar at room temperature was adopted.

A. Shift and width in $\mu^4\mathrm{He}^+$ without fine-structure splitting

We first consider the energy and temperature dependencies of the $2p \to 2s$ spectral line shift and width in $\mu^4\mathrm{He}^+$ calculated without taking into account fine-structure splitting of the $2p$ state. Then the corresponding basis states of the scattering problem are given by

$$\langle \mathbf{r},\mathbf{R}|nl,L:JM\rangle = R_{nl}(r)\sum_{m\lambda}\langle lmL\lambda|JM\rangle Y_{lm}(\hat{\mathbf{r}})Y_{L\lambda}(\hat{\mathbf{R}}). \tag{22}$$

In the case of the $2p$ and $2s$ states Eqs. (17) and (19) are reduced to the following:

$$W^{\rm dip}_{2pL,2sL'}(R) = \left(\delta_{LJ}\hat{L}' + \delta_{L'J}\hat{L}\right)\langle L0L'0|10\rangle I_r\frac{dV_0(R)}{dR}, \tag{23}$$

and

$$\begin{aligned} i\tilde{d}(E) + \frac{\tilde{w}(E)}{2} &= \frac{1}{3}N\frac{\pi}{M_r^2}\sqrt{\frac{M_r}{2E}}\sum_{L,J=L,L\pm1}(2J+1) \\ &\times[1 - \langle 2pL|S^J(E_{2p})|2pL\rangle\langle 2sL|S^L(E_{2s})|2sL\rangle^*]. \end{aligned} \tag{24}$$

In the spinless case, we have a three-channel scattering problem if parity $\pi = (-1)^J$ and a one-channel problem

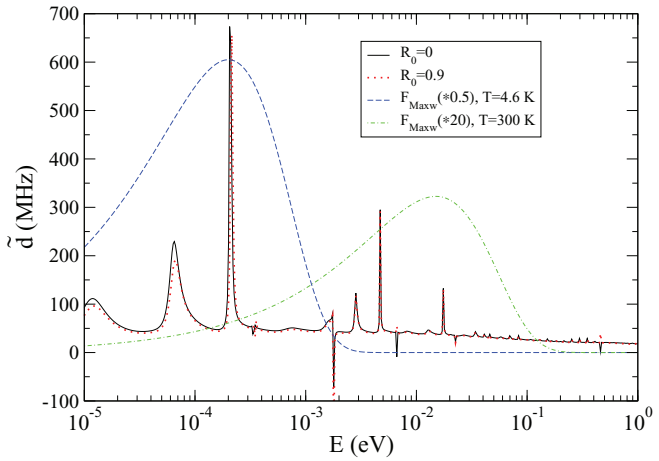

FIG. 3. (Color online) Energy dependence of the collisional shift of the spectral line $2p \rightarrow 2s$ (1.377 eV). Solid line corresponds to the integration of the close-coupling equations starting from $R_0 = 0$; dotted line, from $R_0 = 0.9$ a.u. Dashed and dash-dotted lines illustrate the Maxwellian energy distribution of the target atoms calculated at target temperature 4.6 and 300 K, multiplied by 0.5 and 20, respectively.

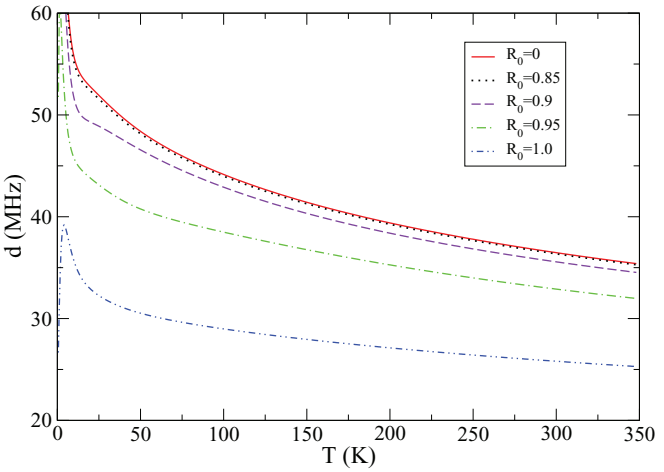

FIG. 4. (Color online) The sensitivity of the collisional shift of the spectral line $2p$-$2s$ (1.377 eV) in μ^4He^+ to the interatomic potential at small distances $R \leqslant 1.0$ a.u. The results obtained by integration starting from different values $R_0 = 0$–1.0 a.u. are shown.

otherwise, while in the case of an explicit account of the fine-structure splitting the scattering problem is a four-channel one at any parity. Below in Figs. 3–6 we present the results of the present study for the energy and temperature dependencies of the collision-induced shift demonstrating both the sensitivity of the pressure shift to the interaction potential and strong closed-channel effect in the case of μ^4He^+. It is noted that the same general features are also true in the case of μ^3He^+.

It is well known that the real ion-atomic potential is usually more repulsive at small R than its approximation by Morse potential. In order to study the sensitivity of our results to the precise details of the interaction potential, the close-coupling equations were numerically solved using different values for the start value R_0 for outward integration (usually to be equal to zero) in the range R from 0 up to 1.0 a.u.

In Fig. 3 the energy dependence of the collisional shift calculated for two values $R_0 = 0$ and $R_0 = 0.9$ is shown. It is seen that the energy dependence of the shift reveals the resonancelike structures associated with a presence of the bound or quasibound rovibronic states, whose positions and widths are quite sensitive to the form and details of the used potential. Comparison of the two variants of the calculations with the different values of R_0 shows that the details of the internal range of the ion-atomic interaction at $R < 0.9$ are practically not important. It is noted that the calculation with $R_0 = 0.9$ in general maintains both the absolute values and complicated structure of the energy dependence shown in Fig. 3 for $R_0 = 0$. Besides, our fit of the *ab initio* potential [22,23] very exactly reproduces the data of the highly accurate quantum-chemistry calculations [22] even for $R = 0.9$ (see Fig. 2).

The Maxwellian energy distribution of the target atoms corresponding to the two values of the target temperature 4.6 and 300 K (the Maxwellian distribution calculated at $T =$ 300 K is multiplied by a factor 20, while at 4.6 K by 0.5) are also plotted in Fig. 3 in order to demonstrate explicitly that averaging over energy in Eq. (20) leads to the smooth dependence of the pressure shift and width on temperature except for the range of very low temperature $T \lesssim 25$ K, as it is shown in Figs. 4–6.

Indeed, since the temperature dependence of the collisional broadening w and shift d at a definite target temperature T is obtained by averaging (19) over energy with the Maxwellian energy distribution of the target atoms, only the resonancelike structures at very low collision energy survive and determine the behavior of both shift and width at the target temperatures below 25 K. At $T > 25$ K we observe the smooth dependence of the shift on temperature: the pressure shift decreases with the increase of temperature.

In Fig. 4 the effect of the short-range repulsion at $R_0 <$ 1.0 is illustrated in more detail. According to our study, the details of the interaction potential in the range $R < 0.85$ are not important, since its total contribution to the pressure shift is less than 0.5%. At the same time, the shift is quite sensitive to the precise details of the potential at $R_0 > 0.85$ (see also Fig. 5). In particular, the shifts calculated with $R_0 = 0.85$ and $R_0 = 1.0$ differ more than 25%. It is worthwhile to emphasize that the observed in Fig. 3 and especially in Fig. 4 sensitivity of the shifts to the variation of the starting point of the outward integration in the classically forbidden range is explained by a significant quantum effect. Indeed, the locations of the inner classical turning point R_{tp} increase from 0.994 ($L = 0$) up to 1.318 ($L = 30$) and from 0.960 ($L = 0$) up to 1.240 ($L = 30$) at collision energies 0.05 and 0.5 eV, respectively. Therefore, the classical or semiclassical approaches are only useful for making crude estimations, however, the results can differ by up to 50% or more in comparison with a rigorous quantum-mechanical description.

The fitted parameter β determines the form (strength) of both the short-range Morse potential $V_M(R)$ (10) and potential of the dipole coupling $V_1(\mathbf{R},\mathbf{r})$ (13). Besides, this parameter changes the relative role of the coupling interaction as compared with the central interaction potential $V_0(R)$ (9). The temperature dependence of the shift calculated at the energy $2p$-$2s$ separation 1.377 eV in μ^4He^+ for three values

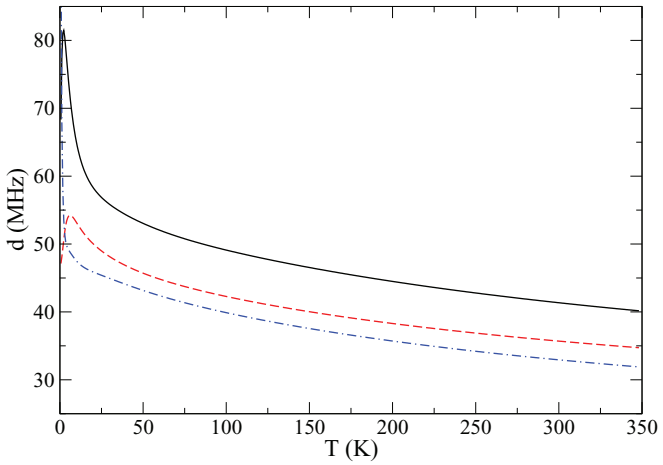

FIG. 5. (Color online) The temperature dependence of the collisional shift $d(T)$ calculated for the energy $2p$-$2s$ splitting 1.377 eV in μ^4He^+ at the different values of Morse potential parameter β: 1.65 (solid line), 1.489 (dashed line), and 1.35 (dash-dotted line).

of the parameter $\beta = 1.35, 1.489$, and 1.65 is plotted in Fig. 5. We observe here the general property: the value of the shift increases with the increase of β.

There are at least two obvious reasons for such effect. First, the increase of β enhances the relative role of the dipole coupling in comparison with the diagonal interaction. Second, since at collisional energies below the $2s$-$2p$ threshold the effect of the closed channels is very important (see Fig. 6), the increase of β leads also to the enhancement of the shift values. In particular, the temperature dependence of the shift plotted in Fig. 6 shows the significant difference between the shift values, obtained with and without taking into account the closed channels. The shift of the spectral lines calculated with the closed channels taken into account, as shown in Fig. 6, are about four times larger than the shift obtained without the closed channels.

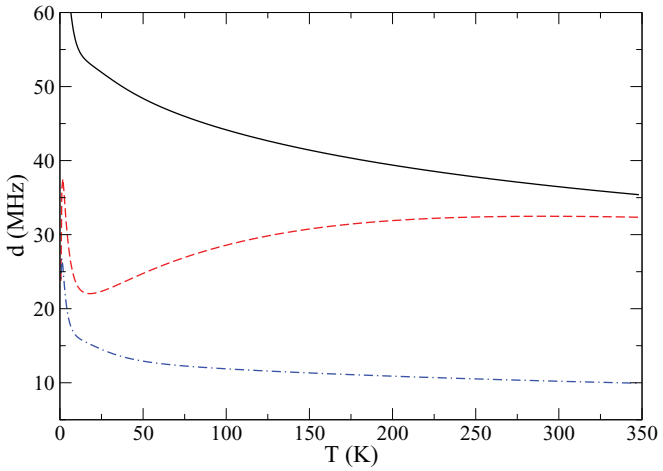

FIG. 6. (Color online) Effect of the long-range interaction $V_p(R)$ and closed channels on the temperature dependence of the collisional shift of the spectral line $2p$-$2s$ (1.377 eV) in μ^4He^+. The solid line corresponds to full calculation, the dashed line to the calculation without V_p, and the dash-dotted line to the calculation without taking into account the closed channels.

It is important to note that, according to the present study, the large contribution to the collisional shift of the spectral lines arises also due to the term in the interaction potential matrix associated with the long-range polarization interaction (see Fig. 6). This contribution is increased and becomes much more pronounced at temperature $T < 150$ K. In particular, at $T = 25$ K the long-range interaction contributes to the total shift about 50%.

B. Fine-structure effect in μ^4He^+

The fine-structure effects on the calculated values of the shift and width arise mainly from the coefficients of the angular momentum coupling ($6j$ symbols) in the interaction matrix potentials Eq. (17) and corresponding dependence of the S-matrix elements due to these interactions. Besides, the scattering problem becomes four channels with two splitting $2p_j$ sublevels as compared with the spinless case.

The effects of the fine-structure splitting on the calculated shift and width values are illustrated respectively in Figs. 7 and 8 in comparison with the case without a fine structure splitting taken into account.

The temperature dependence of the shift calculated at the same value of the $2p$-$2s$ energy level separation is similar in both cases: the shift has a characteristic resonancelike behavior at very small temperature $\lesssim$25 K and tends to decrease slowly with the increase of the target temperature. As a whole the fine-structure effect is not very strong and leads to less than 10% differences of the shift. Thus, the role of the fine-structure splitting is relatively unimportant.

According to the present study, the collisional width of the $2p \to 2s$ spectral lines in average are about an order of magnitude less than the shift. However, the temperature dependencies of both the shift and width are quite similar and have some general features: resonancelike behavior at

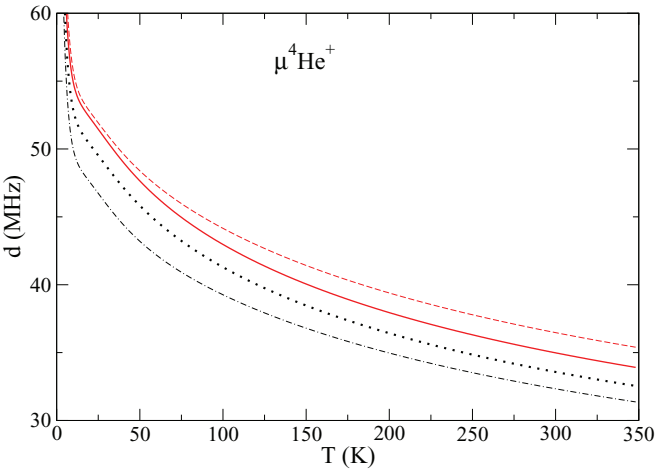

FIG. 7. (Color online) The fine structure effect on the shift of the spectral $2p$-$2s$ lines in in the case of $(\mu^4He)^+_{2l} - ^4$ He collision vs target temperature. The solid and dotted lines show shifts for the lines $2p_{1/2}$-$2s_{1/2}$ (1.377 eV) and $2p_{3/2}$-$2s_{1/2}$ (1.523 eV), respectively. The dashed and dash-dotted lines correspond to the calculations without fine-structure splitting, respectively, for the values 1.377 eV and 1.523 eV of $2p$-$2s$ energy level separation.

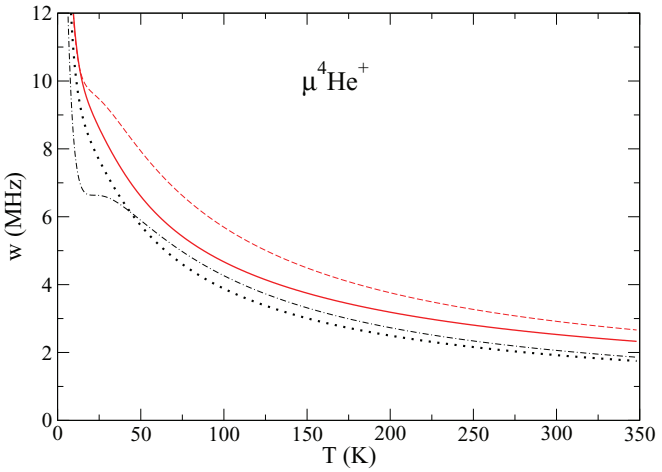

FIG. 8. (Color online) The fine-structure effect on the width in the case of $(\mu^4\mathrm{He})^+_{2l}-{}^4\mathrm{He}$ collision vs target temperature. The designations are the same as in Fig. 7.

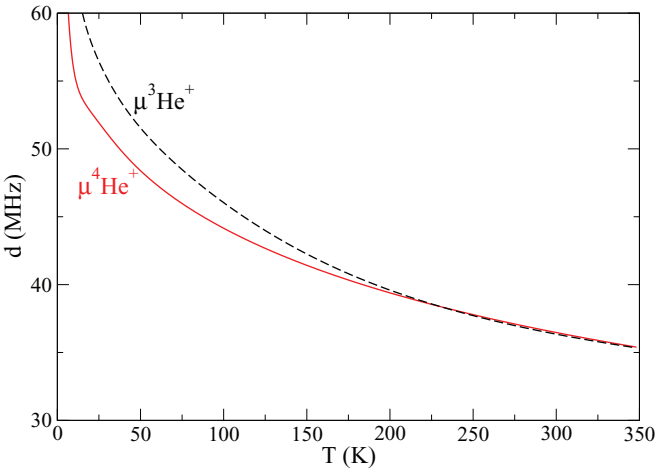

FIG. 9. (Color online) Isotopic effect in the pressure shift: the temperature dependence of the collisional shift of the $2p \to 2s$ spectral lines in $(\mu^4\mathrm{He})^+$ (solid line) and $(\mu^3\mathrm{He})^+$ (dashed line), calculated for the fixed energy level separation is equal to 1.377 eV.

low temperature ($\lesssim$25 K) and decreasing of their values with the increase of the temperature. The fine-structure effect on the width temperature dependence is also revealed and shown in Fig. 8. As in the case of the shift (see Fig. 7), the widths calculated with and without taking into account the fine-structure splitting differ as a whole about 10–15 %. It is noted, that in the range 25–75 K of the target temperature the effect of the fine structure is much stronger.

C. Isotopic effect: Shift and width in $\mu^3\mathrm{He}^+$

The approach developed in the present paper allows us to realize the analogous (as for $\mu^4\mathrm{He}^+$) program of the theoretical study for the case of $\mu^3\mathrm{He}^+$, taking into account also the hyperfine-structure splitting. However, since fine-structure splitting is much larger than hyperfine-structure splitting and, according to the present study, the fine-structure effects are about 10% then we can conclude that the hyperfine-structure effects are negligible for both the shift and width values at the present level of experimental accuracy. Besides, it seems reasonable to assume that the principal results obtained above would be also true for the $2p$-$2s$ spectral lines in the case of $(\mu^3\mathrm{He})^+$. Therefore, now our main interest is to estimate the isotopic effect by comparing, at fixed value of the $2p$-$2s$ energy level splitting, the collisional shift and width of the $2p$-$2s$ spectral lines calculated for $\mu^3\mathrm{He}^+$ and $\mu^4\mathrm{He}^+$. The corresponding results of the present calculations are shown in Figs. 9–10.

To illustrate the isotopic effect, the temperature dependencies of the shift (Fig. 9) and width (Fig. 10) were calculated at fixed value 1.377 eV of the $2p$-$2s$ energy level separation for both $(\mu^3\mathrm{He})^+$ and $(\mu^4\mathrm{He})^+$ without taking into account fine-structure splitting of the $2p$ state.

The isotopic effect for the shift is almost invisible at $T > 200$ K, while at low temperature below 175 K the shift in $(\mu^3\mathrm{He})^+$ is larger than in $(\mu^4\mathrm{He})^+$ and the difference grows with the decrease of the temperature reaching about 8% at 25 K.

Quite the opposite picture of the isotopic effect is observed for the collisional width, especially at target temperature above 100 K. The width in $(\mu^3\mathrm{He})^+$ increases with temperature above 100 K while the width in $(\mu^4\mathrm{He})^+$ decreases with temperature. At $T = 300$ K the width in $(\mu^3\mathrm{He})^+$ is about three times larger than in $(\mu^4\mathrm{He})^+$.

In Fig. 11 we present the temperature dependence of both the collisional shift and width in $(\mu^3\mathrm{He})^+$ calculated for two values of the $2p$-$2s$ energy level separation (1.119 and 1.460 eV) corresponding to the lower and upper physical values, respectively. As it is seen, the temperature dependencies of the shift and width calculated for two values of the energy level separation differ significantly due to large difference of the energy level separation. Such a strong difference in the behavior of the shifts and widths calculated with the energy level separations 1.119 eV and 1.460 eV requires some additional remarks. The effects of the energy splitting between the $2p$ and $2s$ states were considered in the present paper and, according to our study, the influence of the energy splitting

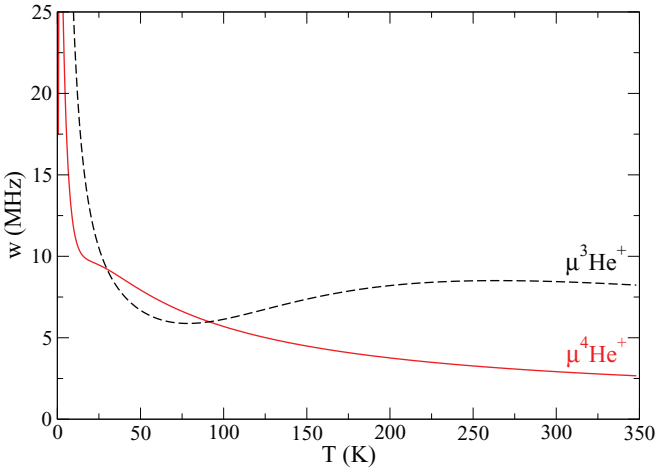

FIG. 10. (Color online) The same as in Fig. 9, but for collisional width. The width of the $2p \to 2s$ spectral lines vs target temperature calculated at the fixed energy level separation 1.377 eV: the solid line for $(\mu^4\mathrm{He})^+$, and dashed line for $(\mu^3\mathrm{He})^+$.

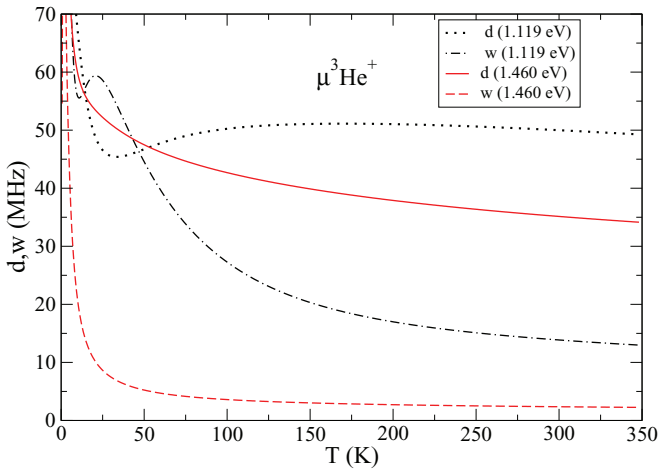

FIG. 11. (Color online) Temperature dependence of the collisional shifts and widths calculated for the spectral line $2p \rightarrow 2s$ of $(\mu^3\mathrm{He})^+$ at two physical values of the $2p$-$2s$ energy level separation 1.119 and 1.460 eV.

can be very strong and results in both the different values and even the different sign of the collisional shift and also changes its temperature dependence. In particular, the decrease of the $2p$-$2s$ energy level separation from 1.460 eV to 1.119 eV, leads to the enhancement of the closed-channel effect, which mainly determines both the shift and width values (see Fig. 6) at collisional energies below the $2s$-$2p$ threshold.

IV. CONCLUSION

The general features of the collisional shifts and broadenings have been studied in a wide range of the collisional energy $E = 10^{-5}$–1 eV and target temperature from 1 up to 350 K. According to the present study, at target density $N = 2.4145 \times 10^{18}$ atom/cm^3 corresponding to the target pressure 100 mbar ($T = 300$ K) the predicted values of the pressure shift of the spectral lines $2p$-$2s$ are equal to 33–35 MHz and 35–50 MHz for $\mu^4\mathrm{He}^+$ and $\mu^3\mathrm{He}^+$, respectively, which is comparable with the systematic uncertainty of the frequency calibration, arising from pulse-to-pulse fluctuations in the laser pulse. At the same conditions the widths are equal to 2.4–13.6 MHz for $\mu^3\mathrm{He}^+$ and 2.0–3.0 MHz for $\mu^4\mathrm{He}^+$.

The present results are very important for the experiments proposed at Paul Scherrer Institute (PSI) aimed at precision measurements of the Lamb $2p$-$2s$ shifts in $\mu^4\mathrm{He}^+$ and $\mu^3\mathrm{He}^+$ ions. In particular, the present predictions of pressure shifts and broadenings of the spectral lines $2p$-$2s$ in $\mu^4\mathrm{He}^+$ and $\mu^3\mathrm{He}^+$ ions give a reliable estimation of their contribution to the systematic uncertainty of the Lamb shift experiments in PSI and allow us to work at much higher gas pressure as compared with muonic hydrogen experiments and, therefore, increase the expected signal rates and also improve statistics.

ACKNOWLEDGMENT

The authors are grateful to Randolf Pohl who called their attention to the importance of the problem and for the useful correspondence concerning this study.

[1] R. Pohl, A. Antognini, F. Nez, F. D. Amaro *et al.*, Nature (London) **466**, 213 (2010).
[2] A. Antognini, F. Biraben, J. M. R. Cardoso, D. S. Covita *et al.*, Can. J. Phys. **89**, 47 (2011).
[3] T. Nebel, F. D. Amaro, A. Antognini, F. Biraben *et al.*, Hyperfine Interact. **212**, 195 (2012).
[4] R. Pohl *et al.*, Phys. Rev. Lett. **97**, 193402 (2006).
[5] V. P. Popov and V. N. Pomerantsev, Phys. Rev. A **83**, 032516 (2011).
[6] H. P. von Arb, F. Dittus, H. Heeb, H. Hofer *et al.*, Phys. Lett. B **136**, 232 (1984).
[7] E. Borie, Ann. Phys. (NY) **327**, 733 (2012).
[8] G. Peach, in *Springer Handbook of Atomic, Molecular, and Optical Physics*, 2nd ed., edited by G. W. F. Drake (Springer, Berlin, 2006), Chap. 59, p. 884.
[9] D. F. T. Mullamphy, G. Peach, V. Venturi, I. B. Whittingham, and S. J. Gibson, J. Phys. B: At. Mol. Opt. Phys. **40**, 1141 (2007).
[10] G. Ya. Korenman, Hyperfine Interact. **119**, 227 (1999).
[11] D. Bakalov, B. Jeziorski, T. Korona, K. Szalewicz, and E. Tchukova, Phys. Rev. Lett. **84**, 2350 (2000).
[12] G. Korenman and S. Yudin, J. Phys.: Conf. Ser. **88**, 012060 (2007).
[13] S. N. Yudin and G. Ya. Korenman, Hyperfine Interact. **209**, 21 (2012).
[14] V. P. Popov and V. N. Pomerantsev, Hyperfine Interact. **138**, 109 (2001).
[15] G. Ya. Korenman, V. N. Pomerantsev, and V. P. Popov, JETP Lett. **81**, 543 (2005).
[16] V. N. Pomerantsev and V. P. Popov, Phys. Rev. A **73**, 040501(R) (2006).
[17] V. N. Pomerantsev and V. P. Popov, JETP Lett. **83**, 273 (2006).
[18] V. N Pomerantsev and V. P. Popov, Hyperfine Interact. **209**, 69 (2012).
[19] V. P. Popov and V. N. Pomerantsev, Phys. Rev. A **86**, 052520 (2012).
[20] R. O. Mueller, V. W. Hughes, H. Rosenthal, and C. S. Wu, Phys. Rev. A **11**, 1175 (1975).
[21] J. S. Cohen and J. N. Bardsley, Phys. Rev. A **23**, 46 (1981).
[22] D. M. Bishop and L. M. Cheung, J. Mol. Spectr. **75**, 462 (1979).
[23] M. Juřek, V. Špirko, and W. P. Kraemer, Chem. Phys. **193**, 287 (1995).
[24] G. Lach, B. Jeziorski, and K. Szalewicz, Phys. Rev. Lett. **92**, 233001 (2004).